Supporting information (SI) for:

What is the nature of interactions of BF_4^-, NO_3^- and ClO_4^- to Cu(II) complexes with Girard's T hydrazine? When can binuclear complexes be formed?

Tanja Keškić,[†] *Božidar Čobeljić,*[†] *Maja Gruden,*[†] *Katarina Anđelković,*[†] *Andrej Pevec,*[‡] *Iztok Turel,*[‡] *Dušanka Radanović**[§] *and Matija Zlatar**[§]

[†]Faculty of Chemistry, University of Belgrade, Studentski trg 12-16, 11000 Belgrade, Serbia.

[‡]Faculty of Chemistry and Chemical Technology, University of Ljubljana, Večna pot 113, 1000 Ljubljana, Slovenia.

[§]Department of Chemistry, Institute of Chemistry, Technology and Metallurgy, National Institute, University of Belgrade, Njegoševa 12, 11000 Belgrade, Serbia.

S1 SUPPORTING INFORMATION FOR X-RAY CRYSTALOGRAPHY

S2 SYNTHESIS OF $[CuLCl]BF_4$ (1) AND $[Cu_2L_2Cl_2](BF_4)_2$ (3) - ADDITIONAL EXPERIMENTAL DETAILS

S3 ADDITIONAL COMPUTATIONAL RESULTS FOR MONONUCLEAR STRUCTURES

S4 ADDITIONAL COMPUTATIONAL RESULTS FOR DIMER STRUCTURES

S1 SUPPORTING INFORMATION FOR X-RAY CRYSTALOGRAPHY

Table S1 Crystal data and structure refinement details for **1**–**3**

	1	**2**	**3**
Formula	$C_{12}H_{18}BClCuF_4N_4O$	$C_{12}H_{18}ClCuN_5O_4$	$C_{24}H_{36}B_2Cl_2Cu_2F_8N_8O_2$
Fw (g mol^{-1})	420.10	395.30	840.21
Crystal size (mm)	0.70×0.65×0.30	0.35×0.15×0.10	0.80×0.40×0.20
Crystal color	green	green	green
Crystal system	monoclinic	monoclinic	monoclinic
Space group	*P* 2$_1$/*c*	*P* 2$_1$/*c*	*P* 2$_1$/*n*
a (Å)	9.9440(4)	10.1820(6)	7.2915(3)
b (Å)	9.3620(4)	8.6362(6)	28.1816(13)
c (Å)	18.5299(7)	18.7170(11)	8.9402(5)
β (º)	95.626(3)	95.178(5)	112.196(6)
V (Å^3)	1716.75(12)	1639.14(19)	1700.95(16)
Z	4	4	2
T (K)	150(2)	293(2)	150(2)
Calcd density (g cm^{-3})	1.625	1.602	1.640
F(000)	852	812	852
No. of collected reflns	16294	7849	15732
No. of independent reflns	3931	3657	3910
R_{int}	0.0361	0.0276	0.0365
No. of reflns observed	3327	2788	3365
No. parameters	249	212	221
$R[I> 2\sigma(I)]^a$	0.0334	0.0346	0.0490
wR_2(all data)^b	0.0858	0.0872	0.1256
Goof , S^c	1.050	1.034	1.107
maximum/minimum residual electron density (e Å^{-3})	+0.63/–0.52	+0.52/–0.44	+1.40/–0.65

$^a R = \sum||F_o| - |F_c||/\sum|F_o|$. $^b wR_2 = \{\sum[w(F_o^2 - F_c^2)^2]/\sum[w(F_o^2)^2]\}^{1/2}$.
$^c S = \{\sum[w(F_o^2 - F_c^2)^2]/(n-p)\}^{1/2}$ where n is the number of reflections and p is the total number of parameters refined.

Table S2 Selected bond lengths (Å) and angles (°) of compounds **1**–**3**

1			
Cu1–N1	2.0023(19)	O1–Cu1–N1	160.64(7)
Cu1–N2	1.9308(18)	O1–Cu1–N2	79.74(7)
Cu1–O1	1.9806(15)	O1–Cu1–Cl1	99.90(5)
Cu1–Cl1	2.2141(6)	N1–Cu1–N2	80.91(8)
N2–N3	1.384(2)	N1–Cu1–Cl1	99.37(6)
O1–C8	1.278(3)	N2–Cu1–Cl1	175.74(6)
2			
Cu1–N1	2.0031(18)	O1–Cu1–N1	159.67(7)
Cu1–N2	1.9239(18)	O1–Cu1–N2	79.59(7)
Cu1–O1	1.9777(15)	O1–Cu1–Cl1	100.03(5)
Cu1–Cl1	2.2056(6)	N1–Cu1–N2	80.65(8)
N2–N3	1.389(2)	N1–Cu1–Cl1	99.06(6)
O1–C8	1.277(3)	N2–Cu1–Cl1	173.50(6)
3			
Cu1–N1	2.023(3)	O1–Cu1–N1	158.68(11)
Cu1–N2	1.931(3)	O1–Cu1–N2	79.80(10)
Cu1–O1	1.977(2)	O1–Cu1–Cl1	99.23(7)
Cu1–Cl1	2.2408(8)	N1–Cu1–N2	80.25(12)
Cu1–Cl1^{i}	2.6800(9)	N1–Cu1–Cl1	98.90(9)
N2–N3	1.373(4)	N2–Cu1–Cl1	168.98(9)
O1–C8	1.285(4)	Cl1–Cu1–Cl1^{i}	94.22(3)

Table S3 Hydrogen-bond parameters for complex **1**

C3-H3···F4	D–H (Å)	H···A (Å)	D···A (Å)	D–H···A (°)	Symm. operation on A
C4-H4···F4	0.95	2.54	3.318(3)	140	1+*x*, *y*, *z*
C7-H7A···F2A[a]	0.95	2.45	3.362(3)	161	2–*x*, 1–*y*, 2–*z*
Intra C11-H11B···F3A[a]	0.98	2.53	3.495(5)	166	2–*x*, –1/2+*y*, 3/2–*z*
Intra C10-H10A···O1	0.98	2.58	3.268(4)	127	
Intra C5-H5···Cl1	0.98	2.27	2.967(3)	127	
C10-H10B···F4	0.95	2.87	3.400(3)	116	
C12-H12A···Cl1	0.98	2.38	3.276(3)	151	*x*, –1+*y*, *z*
C12-H12C···F3A[a]	0.98	2.75	3.662(2)	155	1–*x*, –*y*, 2–*z*
C3-H3···F4	0.98	2.38	3.270(3)	151	1–*x*, –1/2+*y*, 3/2–*z*

[a] Atoms refined with occupation number 0.75.

Table S4 Hydrogen-bond parameters for complex **2**

D–H···A	D–H (Å)	H···A (Å)	D···A (Å)	D–H···A (°)	Symm. operation on A
C2-H2···O2	0.93	2.51	3.375(4)	155	1-*x*, 2-*y*, -*z*
C3-H3···O4	0.93	2.50	3.355(4)	153	-1+*x*, *y*, *z*
Intra C10-H10A···O2	0.96	2.66	3.555(4)	156	
Intra C10-H10A···O1	0.96	2.61	3.195(3)	120	
Intra C11-H11C···O1	0.96	2.30	2.954(3)	125	
Intra C1-H1···Cl1	0.93	2.86	3.377(3)	116	
C12-H12A···O4	0.96	2.51	3.376(4)	150	2-*x*, -1/2+*y*, 1/2-*z*
C12-H12B···Cl1	0.96	2.80	3.680(2)	153	2-*x*, 1-*y*, -*z*
C12-H12C···O4	0.96	2.48	3.377(3)	155	*x*, -1+*y*, *z*

Table S5 Intermolecular π···π interaction parameters for complex **3**

Cg(I)[a]	Cg(J)[a]	Cg(I)-Cg(J)[b] (Å)	α[c] (°)	β[d] (°)	γ[e] (°)	Slippage[f] (Å)	Sym. code on ring (J)
Cg(1)	Cg(1)	3.442(2)	0.03(18)	20.0	20.0	1.176	-1-*x*,-*y*,-*z*
Cg(1)	Cg(1)	3.918(2)	0.03(18)	30.5	30.5	1.991	-*x*,-*y*,-*z*

[a] Labels of aromatic rings (1) = N(1), C(1)-C(5).
[b] Cg(I)-Cg(J) = Distance between ring centroids (Ang.).
[c] α = Dihedral angle between planes (I) and (J) (Deg.).
[d] β = Angle between Cg(I)–Cg(J) vector and normal to plane (I) (Deg.).
[e] γ = Angle between Cg(I) –Cg(J) vector and normal to plane (J) (Deg.).
[f] Slippage = Distance between Cg(I) and perpendicular projection of Cg(J) on ring I (Ang.).

Table S6 Hydrogen-bond parameters for complex **3**

D–H···A	D–H (Å)	H···A (Å)	D···A (Å)	D–H···A (°)	Symm. operation on A
C3-H3···Cl1	0.95	2.75	3.668(4)	162	-1+*x*, *y*, -1+*z*
C4-H4···F3	0.95	2.48	3.313(7)	146	-*x*, -*y*, -*z*
C7-H7A···F2	0.98	2.41	3.231(6)	141	
Intra C11-H11B···N3	0.98	2.47	3.106(6)	122	
C7-H7B···F3	0.98	2.31	3.286(7)	173	-1+*x*, *y*, *z*
C9-H9A···Cl1	0.99	2.77	3.638(4)	147	1-*x*, -*y*, 1-*z*
C9-H9B···F1	0.99	2.46	3.312(6)	144	*x*, *y*, 1+*z*
C10-H10B···F2	0.98	2.26	3.205(6)	162	1/2+*x*, 1/2-*y*, 1/2+*z*
C10-H10C···F1	0.98	2.52	3.413(7)	151	1+*x*, *y*, 1+*z*
C12-H12A···F4	0.98	2.41	3.330(7)	157	*x*, *y*, 1+*z*
Intra C12-H12B···N3	0.98	2.42	3.047(5)	121	

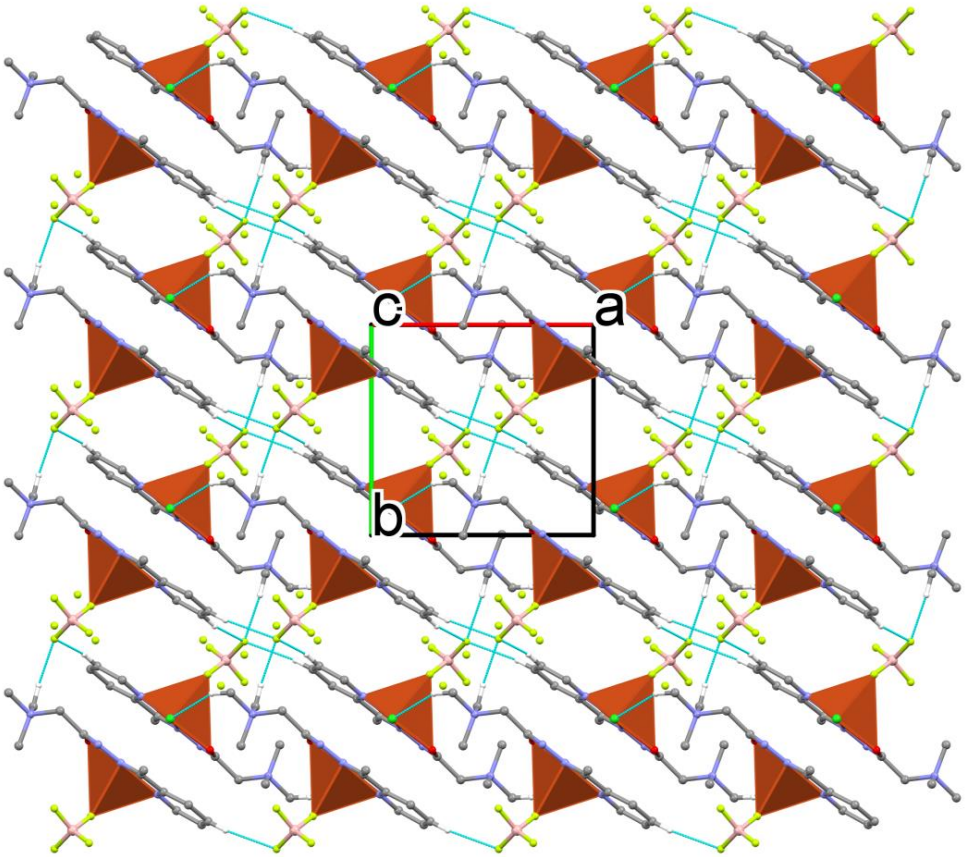

Figure S1 A view of the crystal packing of **1** showing complex molecules connected by means of C-H···F and C-H···Cl hydrogen bonds (dashed blue lines) into layer parallel with the (0 0 1) lattice plain. Hydrogen atoms have been omitted for the sake of clarity, except those involved in hydrogen bonding.

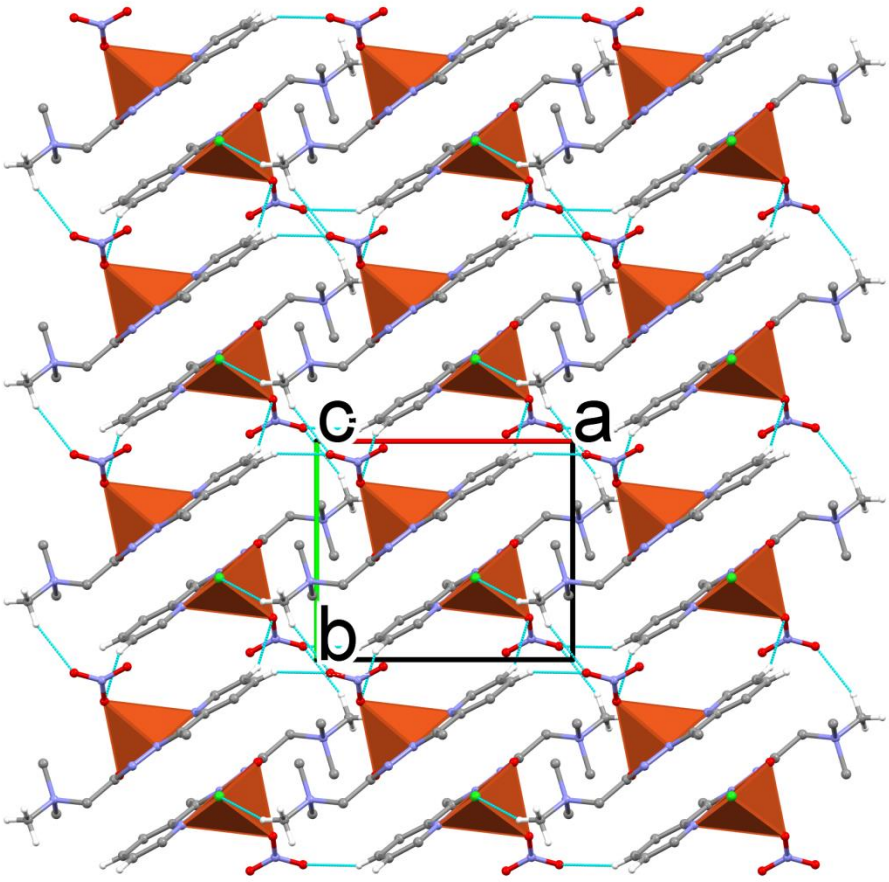

Figure S2 A view of the crystal packing of **2** showing complex molecules connected by means of C-H···O(nitrate) and C-H···Cl hydrogen bonds (dashed blue lines) into layer parallel with the (001) lattice plain. Hydrogen atoms have been omitted for the sake of clarity, except those involved in hydrogen bonding.

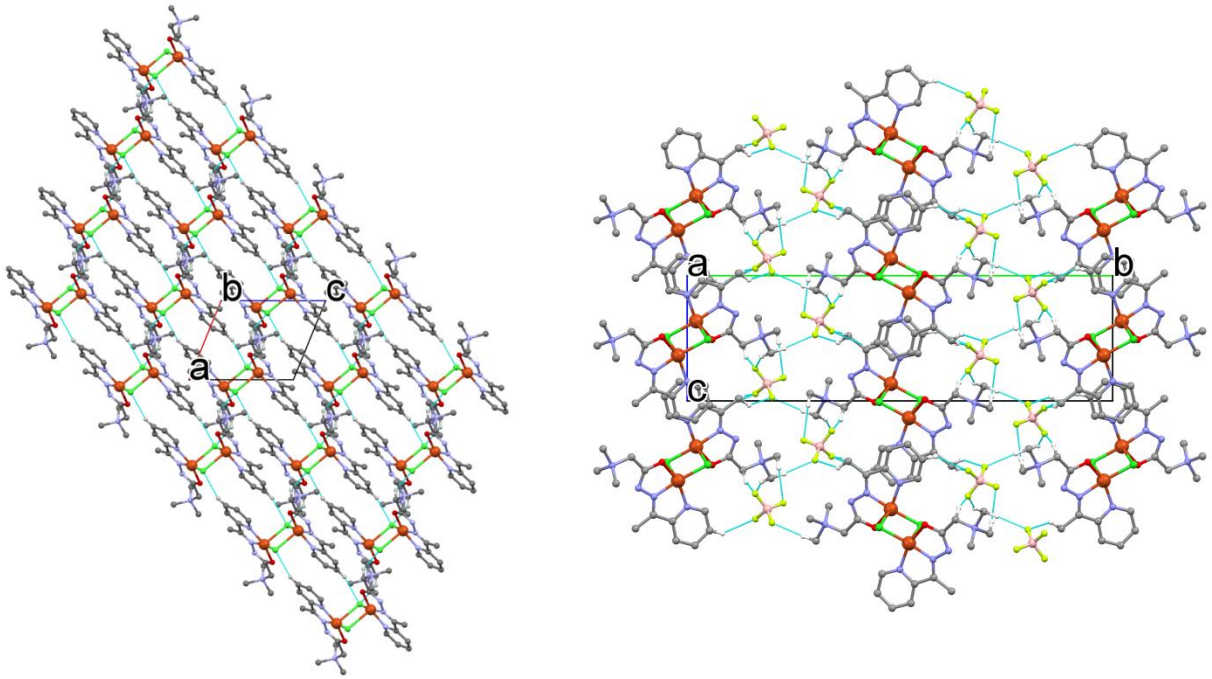

a) b)

Figure S3 a) A view along the *b* axis of **3** showing dimeric complex molecules joined into layer parallel with the (010) lattice plane by π···π stacking interactions between the aromatic rings and C-H···Cl hydrogen bonds; b) Side view of the layers parallel with the (010) showing the function of the BF_4^- anions in the crystal structure of **3**. Hydrogen atoms have been omitted for the sake of clarity, except those involved in hydrogen bonding.

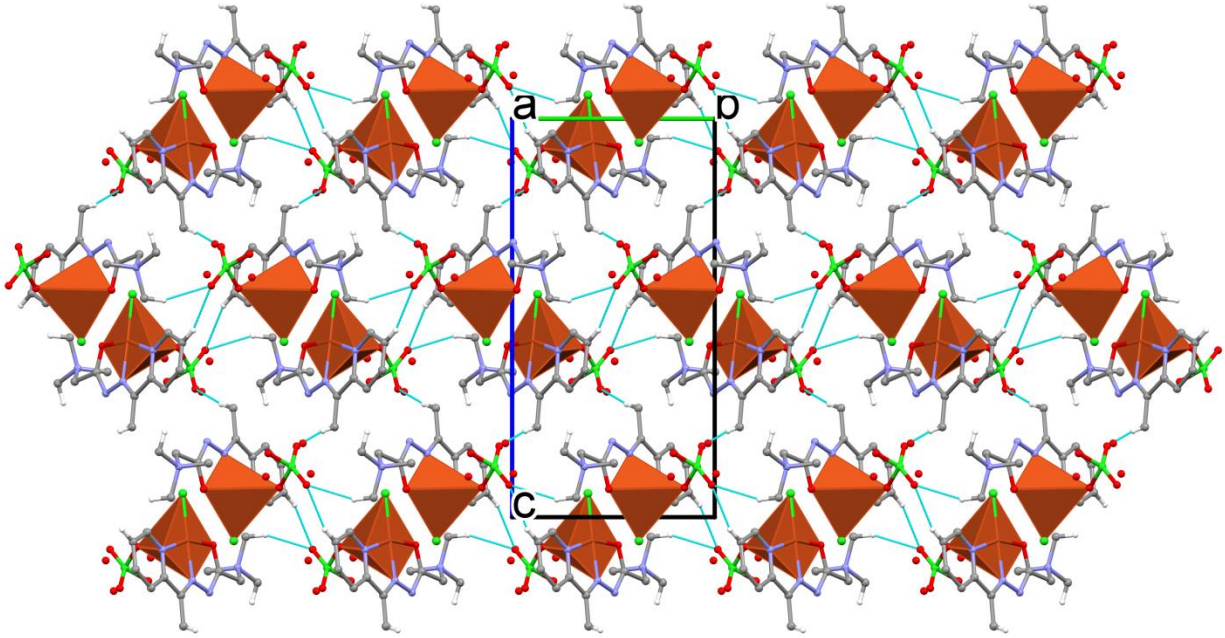

Figure S4 A view of (1 0 0) layer showing complex molecules of **4**[1] connected by means of C-H···O(perchlorate) hydrogen bonds (dashed blue lines). Hydrogen atoms have been omitted for the sake of clarity, except those involved in hydrogen bonding.

S2 SYNTHESIS OF [CuLCl]BF_4 (1) AND $[Cu_2L_2Cl_2](BF_4)_2$ (3) - ADDITIONAL EXPERIMENTAL DETAILS

In order to favorize the formation of mono- or binuclear Cu(II) complex series of reactions were performed. In the reaction of the H**L**Cl ligand with $Cu(BF_4)_2 \cdot 6H_2O$ different molar ration were applied, 1: 1, 1 : 2, 1 : 4 and 2 : 1. Each reaction was done in water, ethanol, acetonitrile, mixture of acetonitrile : methanol or acetonitrile : water. All these reactions were refluxed at different periods of time (30 min, 1 h, 3 h and 5 h). In every case the mixture of mono- and binuclear Cu(II) complexes (**1** and **3**) were obtained.

S3 ADDITIONAL COMPUTATIONAL RESULTS FOR MONONUCLEAR STRUCTURES

Table S7. Energy decomposition analysis at different levels of theory of $[Cu\mathbf{L}Cl]^{+}$-- BF_4^- in monomer structure **1** (**1**--BF_4^-) with F atoms optimized; energy components are given in kcal/mol; Δq is Hirshfeld charge, transferred between fragments.

$[Cu\mathbf{L}Cl]^{+}$-- BF_4^-	Energy Component	BP86-D3	PBE-D3	revPBE-D3	M06L-D3
	E_{elst}	-63.64	-64.04	-64.26	-63.29
	E_{Pauli}	11.95	9.61	13.14	4.06
	E_{orb}	-13.05	-13.07	-13.12	-14.23
	E_{disp}	-5.55	-3.27	-5.95	-0.77
	E_{int}	-70.29	-70.78	-70.19	-74.23
	Δq	0.07	0.07	0.07	0.07

Table S8. Energy decomposition analysis at different levels of theory of $[Cu\mathbf{L}Cl]^{+}$-- ClO_4^- in monomer structure **4** (**4**--ClO_4^-); coordinates of all atoms are taken from the X-ray structure of **4**; energy components are given in kcal/mol; Δq is Hirshfeld charge, transferred between fragments.

$[Cu\mathbf{L}Cl]^{+}$-- BF_4^-	Energy Component	BP86-D3	PBE-D3	revPBE-D3	M06L-D3
	E_{Pauli}	-63.2	-63.48	-63.67	-63.01
	E_{orb}	11.05	8.72	12.08	3.06
	E_{disp}	-20.92	-21.21	-21.14	-19.49
	E_{int}	-8.37	-4.83	-8.74	-1.03
	Δq	-81.45	-80.8	-81.47	-80.46

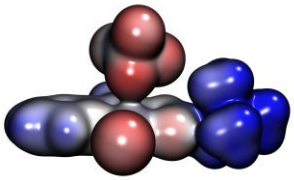

a)

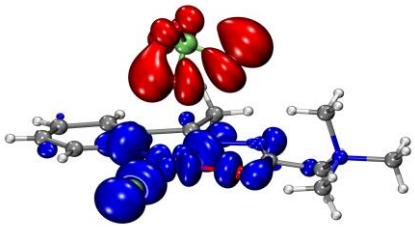

b) ΔE = -8.99 kcal/mol

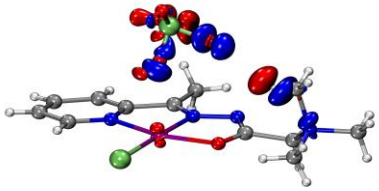

c) ΔE = -0.91 kcal/mol

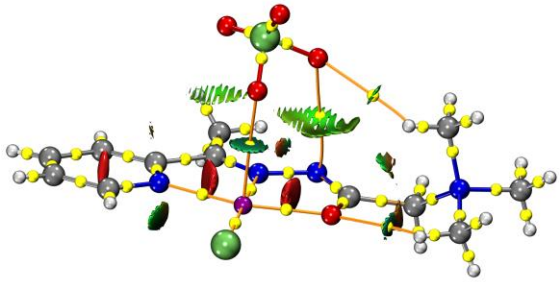

d)

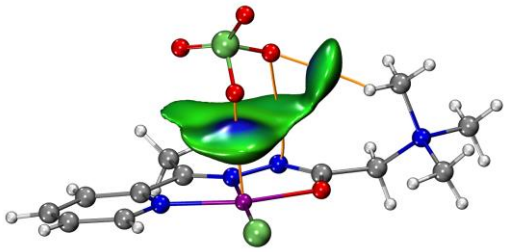

e)

Figure S5 a) Electrostatic potential surfaces (at 0.01 au) from −0.13 (red) to +0.13 (blue) a.u. of monomeric units **4**--ClO_4^-. b) and c) Most important covalent deformation density channels from NOCV analysis of **4**--ClO_4^-. d) Three dimensional NCI plots for **4**--ClO_4^-; isosurfaces (isovalue s=0.4) are colored in range -0.03<sign(λ2)*ρ<0.02 ("Blue-Green-Red" color scheme). Bond paths, connecting bond critical points (yellow spheres) and nuclear critical points (coinciding with atoms) are shown as orange lines. e) IGM plots for **4**--ClO_4^-; isosurfaces of δg^{inter} (isovalue 0.004) colored by sign(λ2)*ρ (range -0.05 to 0.05, "Blue-Green-Red" color scheme). Coordinates of all atoms are taken from the X-ray structure of **4.**

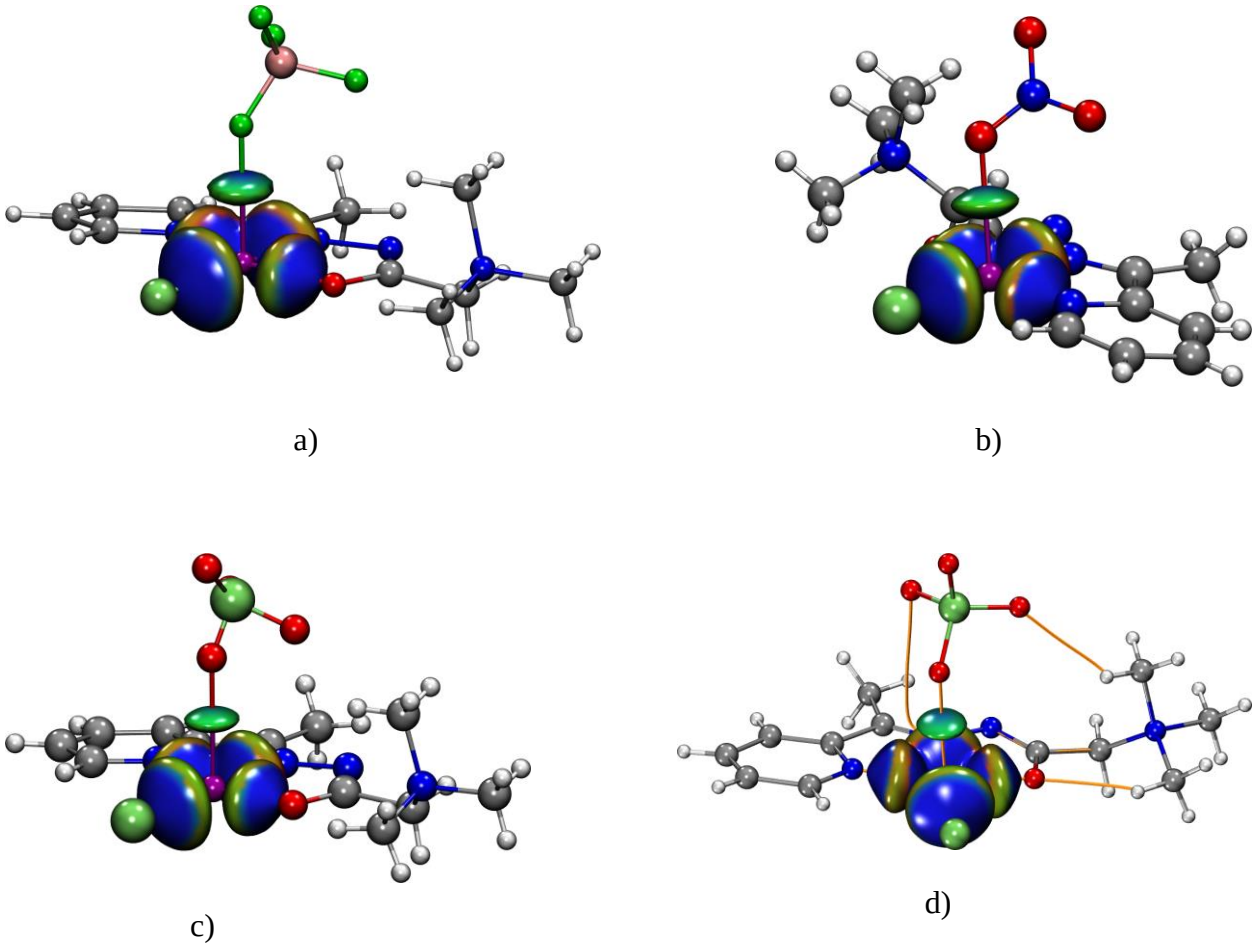

Figure S6 IGM plots around Cu(II) ion for a) **1**--BF_4^- b) **2**--NO_3^- c) **4**--ClO_4^- (all atoms from X-ray) d) **4**--ClO_4^- (O(perchlorate) atoms optimized); isosurfaces of δg^{inter} (isovalue 0.01) colored by sign(λ_2)*ρ (range -0.05 to 0.05).

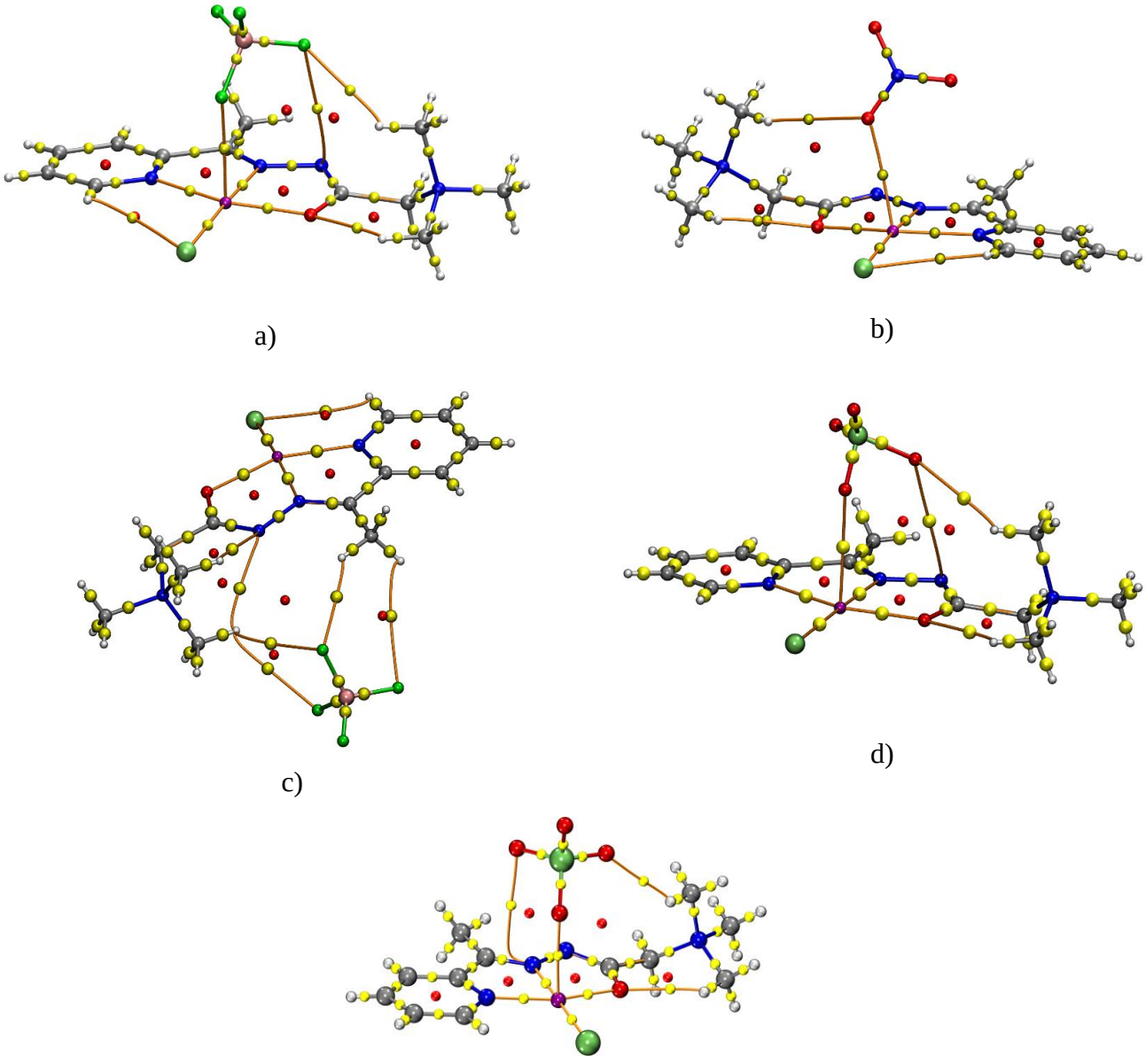

Figure S7 QTAIM topology maps for: a) **1**--BF_4^- b) **2**--NO_3^- c) **3**--BF_4^- d) **4**--ClO_4^- (all atoms from X-ray) e) **4**--ClO_4^- (O(perchlorate) atoms optimized). Bond critical points are depicted as yellow spheres, ring critical points as red spheres, nuclear critical points coincide with atoms. Bond paths connecting bond critical points and nuclear critical points are shown as orange lines.

Table S9 The topological properties of the electron density in interfragment bond critical points in structures **1**, **2**, **3** and **4**: The electron density, $\rho(r_c)$, its Laplacian, $\nabla^2(r_c)$, total energy density, $H(r_c)$, the potential energy density, $V(r_c)$ the kinetic energy density, $G(r_c)$, ellipticity, $\varepsilon(r_c)$, δg index (all in a.u.). Ratio $|V(r_c)|/G(r_c)$ is indicating covalent character. Estimation of the interaction energy of a contact $E_{int}=1/2V(r_c)$ in kcal/mol.

Molecule	Contact	$\rho(r_c)$	$\nabla^2(r_c)$	$H(r_c)$	$V(r_c)$	$G(r_c)$	$\lvert V(r_c)\rvert/G(r_c)$	$\varepsilon(r_c)$	$\delta g(r_c)$	E_{int}
1	Cu--F1A	0.0186	0.0772	0.0018	-0.0158	0.0175	0.90	0.0124	0.0345	-4.95
	F2--HC11	0.0063	0.0253	0.0014	-0.0035	0.0049	0.71	0.0684	0.0115	-1.09
	F2--N3	0.0029	0.0107	0.0007	-0.0013	0.0020	0.65	1.0795	0.0046	-0.43
2	Cu--O2	0.0213	0.0730	0.0005	-0.0172	0.0177	0.98	0.0822	0.0335	-5.40
	O2--HC10	0.0061	0.0207	0.0012	-0.0028	0.0040	0.70	0.1260	0.0091	-0.88
3	F2--HC7	0.0025	0.0098	0.0006	-0.0013	0.0019	0.68	1.5713	0.0048	-0.40
	F1--HC7	0.0087	0.0359	0.0030	-0.0049	0.0069	0.71	0.0387	0.0168	-1.55
	F2--HC12	0.0048	0.0183	0.0010	-0.0026	0.0036	0.72	0.0881	0.0087	-0.82
	F3--HC12	0.0042	0.0161	0.0009	-0.0023	0.0031	0.74	0.3359	0.0081	-0.71
4	Cu--$OClO_4$	0.0148	0.0517	0.0007	-0.0115	0.0122	0.94	0.0299	0.0279	-3.61
	O--Nm	0.0067	0.0276	0.0016	-0.0038	0.0053	0.72	0.0703	0.0139	-1.18
	O--N	0.0039	0.0158	0.0010	-0.0019	0.0029	0.65	0.8216	0.0070	-0.61
4(O-opt)[a]	Cu--$OClO_4$	0.0155	0.0485	0.0004	-0.0112	0.0117	0.96	0.0410	0.0243	-3.52
	O--Nm	0.0077	0.0060	0.0017	-0.0043	0.0061	0.71	0.0530	0.0156	-1.36
	O--N	0.0033	0.1120	0.0007	-0.0013	0.0021	0.65	1.0348	0.0049	-0.47

[a]O atoms of ClO_4^- optimized.

S4 ADDITIONAL COMPUTATIONAL RESULTS FOR DIMER STRUCTURES

Table S10. Energy decomposition analysis at different levels of theory of [Cu**L**Cl]-- [Cu**L**Cl] dimeric structure of **1** with F atoms optimized; energy components are given in kcal/mol; Δq is Hirshfeld charge, transferred between fragments.

[Cu**L**ClX]--[Cu**L**ClX]	Energy Component	BP86-D3	PBE-D3	revPBE-D3	M06L-D3
(BF_4^-)**1**--**1**(BF_4^-)	E_{elst}	-20.13	-20.65	-20.56	-18.18
	E_{Pauli}	32.31	28.64	35.01	13.59
	E_{orb}	-15.49	-15.54	-15.20	-18.18
	E_{disp}	-21.50	-12.11	-21.66	-2.93
	E_{int}	-24.80	-19.67	-22.41	-25.70
	Δq	0.00	0.00	0.00	0.00

Table S11. Energy decomposition analysis at different levels of theory of [Cu**L**Cl]-- [Cu**L**Cl] dimeric structure of **4**; coordinates of all atoms are taken from the X-ray structure of **4**; energy components are given in kcal/mol; Δq is Hirshfeld charge, transferred between fragments.

[Cu**L**ClX]--[Cu**L**ClX]	Energy Component	BP86-D3	PBE-D3	revPBE-D3	M06L-D3
(ClO_4^-)**4**--**4**(ClO_4^-)	E_{elst}	-18.93	-19.4	-19.30	-17.06
	E_{Pauli}	33.79	30.27	36.32	16.16
	E_{orb}	-16.21	-16.30	-15.98	-18.52
	E_{disp}	-20.49	-11.55	-20.51	-2.94
	E_{int}	-21.84	-16.98	-19.47	-22.35
	Δq	0.00	0.00	0.00	0.00

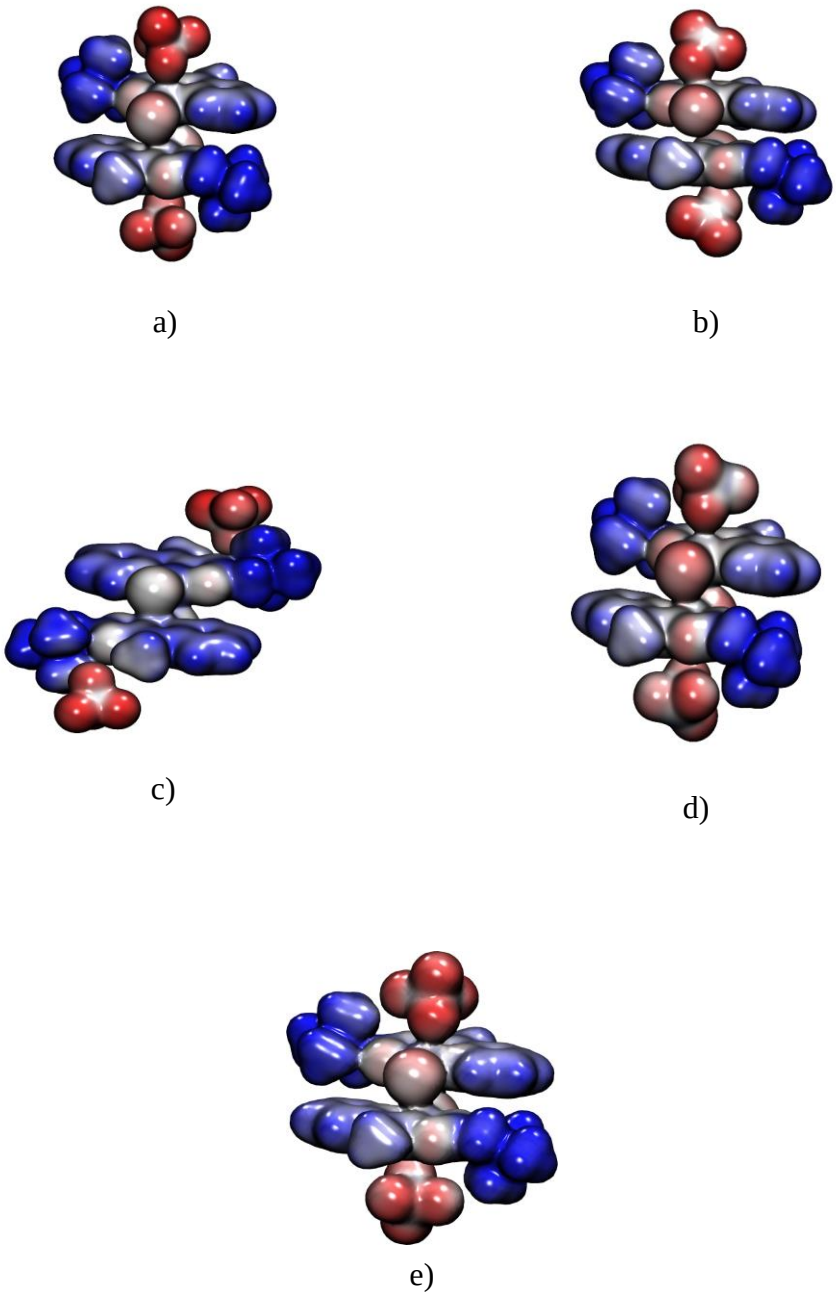

Figure S8 Electrostatic potential surfaces (at 0.01 au) from −0.13 (red) to +0.13 (blue) a.u. of dimer structures a) **1**--**1** b) **2**--**2** c) **3** d) **4**--**4** (all atoms from X-ray) e) **4**--**4** (O(perchlorate) atoms optimized)

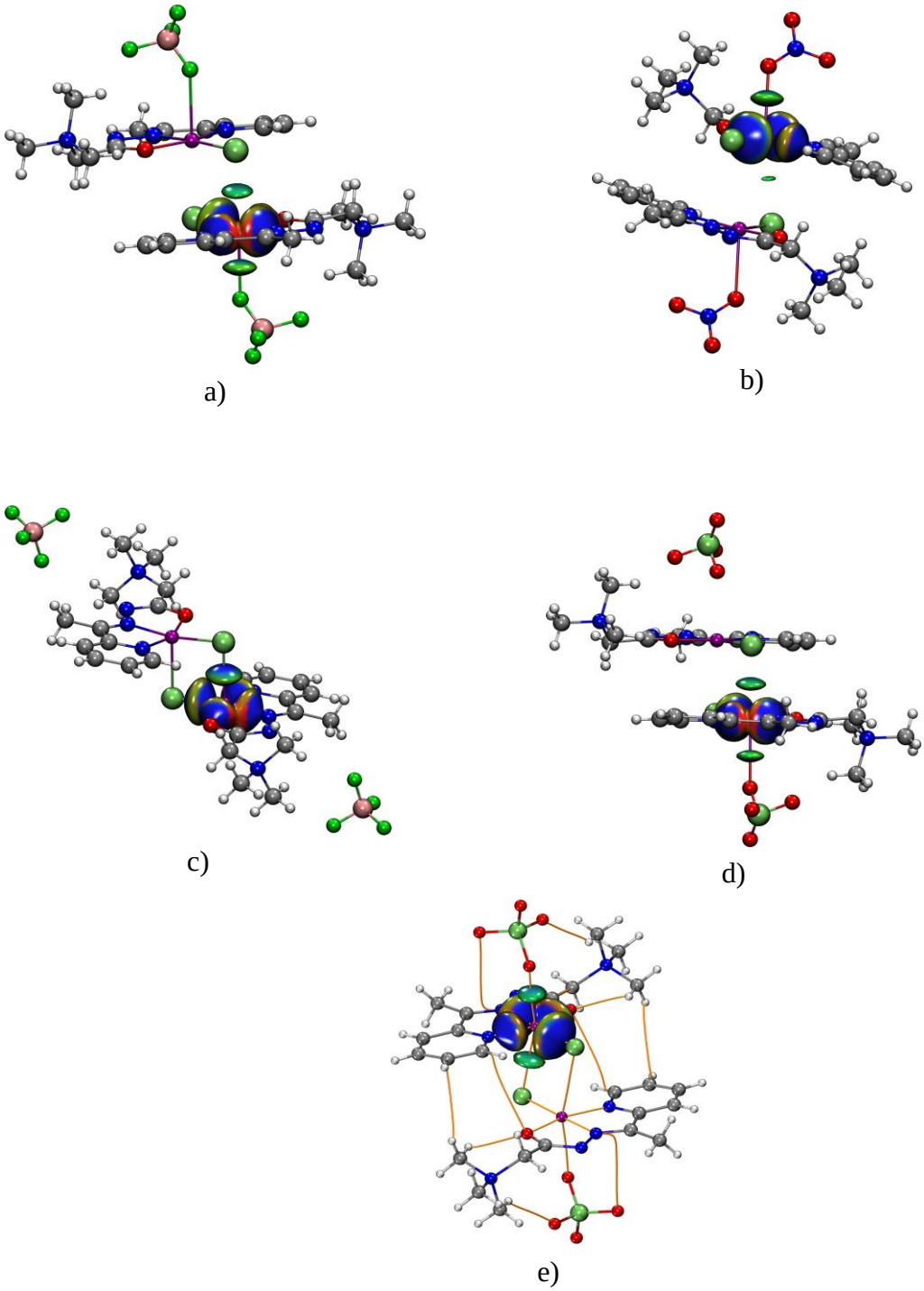

Figure S9 IGM plots around Cu(II) ion for a) **1**--**1** b) **2**--**2** c) **3** d) **4**--**4** (all atoms from X-ray) e) **4**--**4** (O(perchlorate) atoms optimized); isosurfaces of δg^{inter} (isovalue 0.01) colored by sign(λ_2)*ρ (range -0.05 to 0.05). Because of symmetry, isosurfaces are shown only around one Cu.

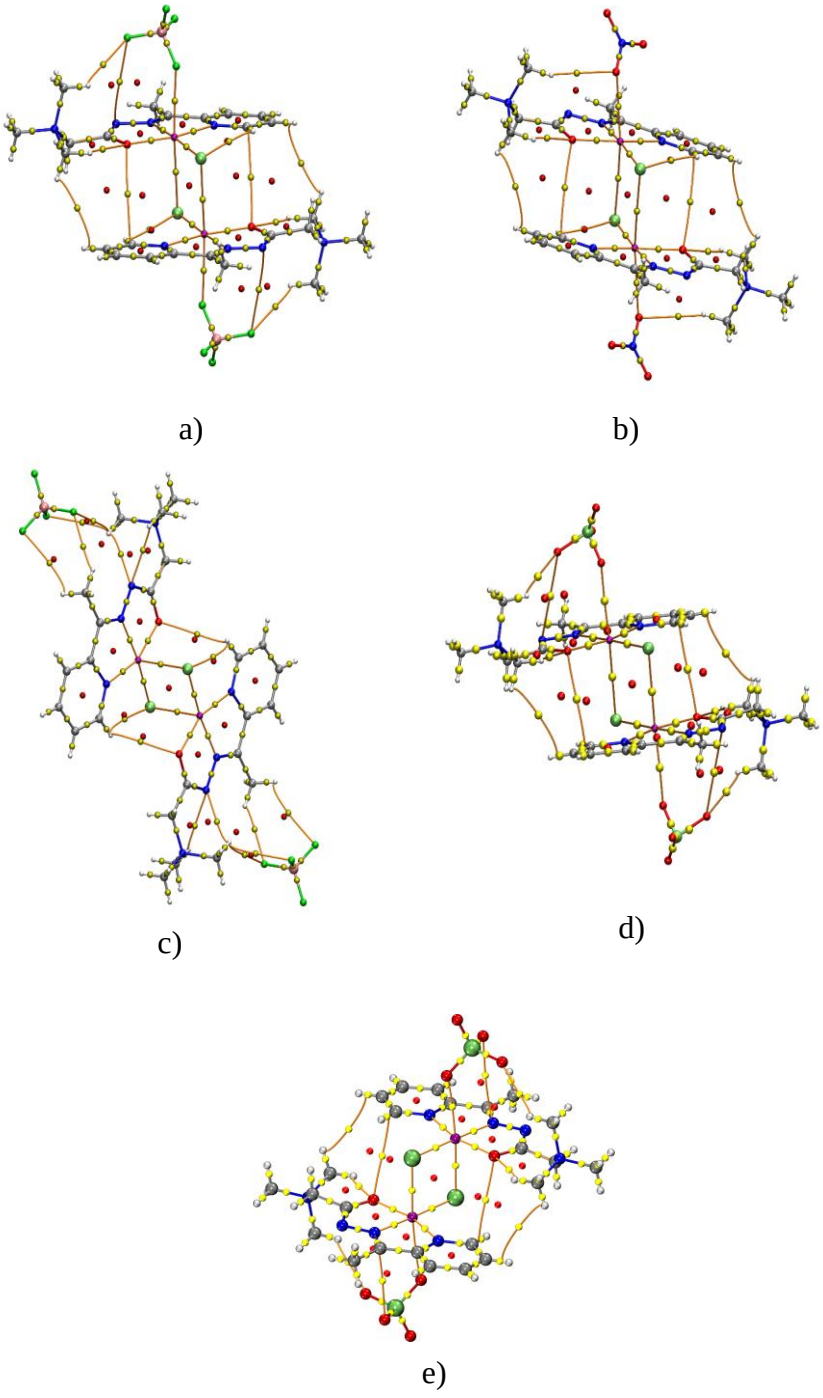

Figure 10 QTAIM topology maps for a) **1--1** b) **2--2** c) **3** d) **4--4**. Bond critical points are depicted as yellow spheres, ring critical points as red spheres, nuclear critical points coincide with atoms. bond paths connecting bond critical points and nuclear critical points are shown as orange lines.

Table S12 The topological properties of the electron density in interfragment bond critical points in dimeric structures of **1**, **2**, **3** and **4**: The electron density, $\rho(r_c)$, its Laplacian, $\nabla^2(r_c)$, total energy density, $H(r_c)$, the potential energy density, $V(r_c)$ the kinetic energy density, $G(r_c)$, ellipticity, $\varepsilon(r_c)$, δg index (all in a.u.). Ratio $|V(r_c)|/G(r_c)$ is indicating covalent character. Estimation of the interaction energy of a contact $E_{int}=1/2V(r_c)$ in kcal/mol.

Molecule	Contact	$\rho(r_c)$	$\nabla^2(r_c)$	$H(r_c)$	$V(r_c)$	$G(r_c)$	$\lvert V(r_c)\rvert/G(r_c)$	$\varepsilon(r_c)$	$\delta g(r_c)$	E_{int}
1--**1**	Cu--Cl^{i}	0.0168	0.0384	-0.0006	-0.0108	0.0102	1.06	0.0905	0.0241	-3.39
	C2H--C10^{i}H	0.0035	0.0123	0.0007	-0.0016	0.0023	0.70	0.7159	0.0105	-0.49
	C1--O1^{i}	0.0029	0.0096	0.0006	-0.0012	0.0018	0.67	0.2431	0.0049	-0.38
2--**2**	Cu--Cl^{i}	0.0104	0.0218	-0.0002	-0.0058	0.0056	1.04	0.1150	0.0148	-1.84
	C2H--C11^{i}H	0.0027	0.0099	0.0006	-0.0012	0.0018	0.67	1.2122	0.0085	-0.36
	C1--O1^{i}	0.0032	0.0106	0.0007	-0.0013	0.0020	0.65	0.5279	0.0059	-0.42
3--**3**	Cu--Cl^{i}	0.0313	0.0953	-0.0016	-0.0271	0.0255	1.06	0.0295	0.0497	-8.50
	O1--C5^{i}H	0.0029	0.0108	0.0007	-0.0014	0.0020	0.70	0.3724	0.0052	-0.42
4--**4**	Cu--Cl^{i}	0.0182	0.0431	-0.0006	-0.0121	0.0114	1.06	0.0682	0.0263	-3.78
	C2H--C10^{i}H	0.0025	0.0094	0.0006	-0.0011	0.0017	0.65	1.1380	0.0079	-0.34
	C1--O1^{i}	0.0027	0.0095	0.0006	-0.0012	0.0018	0.67	0.3118	0.0048	-0.36
4--**4** (O-opt)[a]	Cu--Cl^{i}	0.0182	0.0432	-0.0006	-0.0120	0.0114	1.05	0.0671	0.0261	-3.75
	C2H--C10^{i}H	0.0026	0.0094	0.0006	-0.0011	0.0017	0.65	1.1413	0.0080	-0.34
	C1--O1^{i}	0.0028	0.0095	0.0006	-0.0012	0.0018	0.65	0.3023	0.0048	-0.36

[a]O atoms of ClO_4^- optimized.

REFERENCES

1 M. R. Milenković, A. T. Papastavrou, D. Radanović, A. Pevec, Z. Jagličić, M. Zlatar, M. Gruden, G. C. Vougioukalakis, I. Turel, K. Anđelković and B. Čobeljić, *Polyhedron*, 2019, **165**, 22–30.